Geotech Geol Eng (2012) 30:991–1011
DOI 10.1007/s10706-012-9522-5

ORIGINAL PAPER

Evaluating Kinematic Controls on Planar Translational Slope Failure Mechanisms Using Three-Dimensional Distinct Element Modelling

Marc-André Brideau · Doug Stead

Received: 13 May 2011 / Accepted: 14 May 2012 / Published online: 27 May 2012

Abstract This paper investigates the importance of kinematic release mechanisms on planar translational slope failure using three-dimensional distinct element codes. The importance of the dip and dip direction of the rear, basal and lateral release surfaces and their influence on failure mechanism, dilation, and the development of step-path failures is illustrated. The three-dimensional block shape and volume of the unstable rock masses simulated with the different discontinuity set geometries are characterized. Two assumed three-dimensional slope models are investigated in order to assess the importance of varying kinematic confinement/release mechanisms. These two assumed boundary conditions are shown to be critical in the development of asymmetrical rock mass deformation patterns. Scale effects due to the block size and discontinuity persistence are shown to control the calculated displacement and failure mechanisms. The numerical modelling results are also demonstrated to be sensitive to the assumed normal and shear stiffness of the discontinuities. The influence of the factors investigated on the failure of a single rock block versus a rock mass are compared and discussed.

M.-A. Brideau (✉)
University of Auckland, 23 Symonds Street, Private Bag 92019, Auckland 1142, New Zealand
e-mail: m.brideau@auckland.ac.nz

D. Stead
Simon Fraser University, 8888 University Drive, Burnaby, BC V5A 1S6, Canada

Keywords Slope stability · Distinct element modelling · Rock mechanics · Kinematics

1 Introduction

The first stage in assessing feasible failure mechanisms in a rock slope is typically a kinematic analysis. This method provides a rapid and easy preliminary analysis and an appropriate and necessary starting point. Limitations of this technique include a lack of consideration of block size or shape and the presence and influence of interactions between multiple discontinuity sets. Using a three-dimensional distinct element code, this paper investigates the influence on rock slope failure mechanism of the:

1. Dip direction and dip angle of the rear release discontinuity set
2. Dip direction and dip angle of the lateral release discontinuity set
3. Dip direction of the basal surface discontinuity set
4. Block size
5. Persistence of the discontinuity
6. Degree of kinematic confinement in three-dimensions

Based on kinematic analysis alone, all the discontinuity set geometries investigated in this paper would indicate planar translational sliding. A similar investigation on the controls on block toppling using three-dimensional distinct element code was performed by

Brideau and Stead (2010) and Cheng et al. (2010). Preliminary results from the current planar sliding investigation were presented in Brideau and Stead (2009).

Planar sliding was selected as the primary failure mechanism investigated in this paper, since it is the simplest rock slope failure mode and because "sliding along an adversely orientated rock face or block edge will invariably occur if the kinematic conditions for such sliding are met" (Goodman and Kieffer 2000). A sliding mechanism (on one- or two-planes) will be favoured over rotational movement if the geometry allows for a finite and removable block to form (Goodman 2003; Goodman and Kieffer 2000).

The sensitivity of the failure mechanism to the orientation of a pair of discontinuity sets has been previously investigated by Kimber et al. (1998). In their study they used a two-dimensional distinct element code and varied the dip angle of the basal discontinuity set while keeping the dip angle of the rear release discontinuity constant. The failure mechanism was demonstrated to vary between sliding, sliding/toppling and toppling for different combinations of discontinuity orientation. They also varied the aspect ratio of the blocks to show its influence on the failure mechanism (Kimber et al. 1998). The present study investigates blocks with a different aspect ratio using a three-dimensional distinct element model.

2 Numerical Modelling

The three-dimensional distinct element code 3DEC (Itasca 2008) is used in this paper due to its ability to model large displacement and rotation along block boundaries allowing failure mechanisms such as sliding and toppling to be modeled efficiently. The characteristics of a rigid, elastic, or deformable material type can be defined by the user. The strength along the block boundaries (discontinuities) can also be specified. Additional information concerning the theory behind 3DEC can be found in Cundall (1988), Hart et al. (1988) and Hart (1993). In order to focus on the kinematic controls on rock slope stability, two simple conceptual slope topographies with rigid blocks and the same shear strength parameters on all discontinuities were assumed in the models presented in this paper. Table 1 lists the assumed rock density and the discontinuity properties used in the three-dimensional distinct element models.

Table 1 Rock density and joint properties used in the 3DEC models

Material property	
Density (kg/m^3)	2,700
Joint properties	
Shear stiffness (GPa/m)	1
Normal stiffness (GPa/m)	5
Friction angle (°)	29
Cohesion (MPa)	0
Tensile strength (MPa)	0

The reference discontinuity set geometry (all three mutually perpendicular) assumed in the 3DEC models consisted of a basal discontinuity with an orientation of 30°/270° (dip/dip direction), a rear release discontinuity of 60°/090°, and a lateral release discontinuity of 90°/000°. Figure 1a and 1b present the two assumed slope profiles investigated. The first model (model 1) consists of a two-dimensional cross-section that is susceptible to sliding (i.e. daylighting basal discontinuity and perpendicular rear release surface) extended 100 m in the third dimension and bounded by assumed vertical and fixed lateral boundaries. The second 3DEC model (model 2), has the same longitudinal cross-section but its lateral boundaries are assumed to be sloping and free. These two 3DEC geometries were investigated simulate the various levels of lateral kinematic confinement found in rock slopes. In the present conceptual study it was assumed that no imposed stresses were present along the model boundaries. Figure 2a presents a natural slope example where kinematic confinement is present at both sidescarps of the failure, while in Fig. 2b a gully results in one of the lateral boundaries being kinematically free. The discontinuity spacing (block size) for the two three-dimensional models was varied between 1, 2, 3 m; 6, 12, 18 m; and 6, 12, 18 m on the basal, lateral release and rear release discontinuities, respectively in order to investigate the effect of scale effects on the calculated displacement values and failure mechanisms. This led to a constant block aspect ratio of (height: width: length) 1:6:6 and a tabular block shape. The block aspect ratio was chosen to favour a simple sliding failure mechanism according to the block shape stability charts proposed by Ashby (1971), Bray and Goodman (1981), Choquet and Tanon (1985), and Sagaseta (1986).

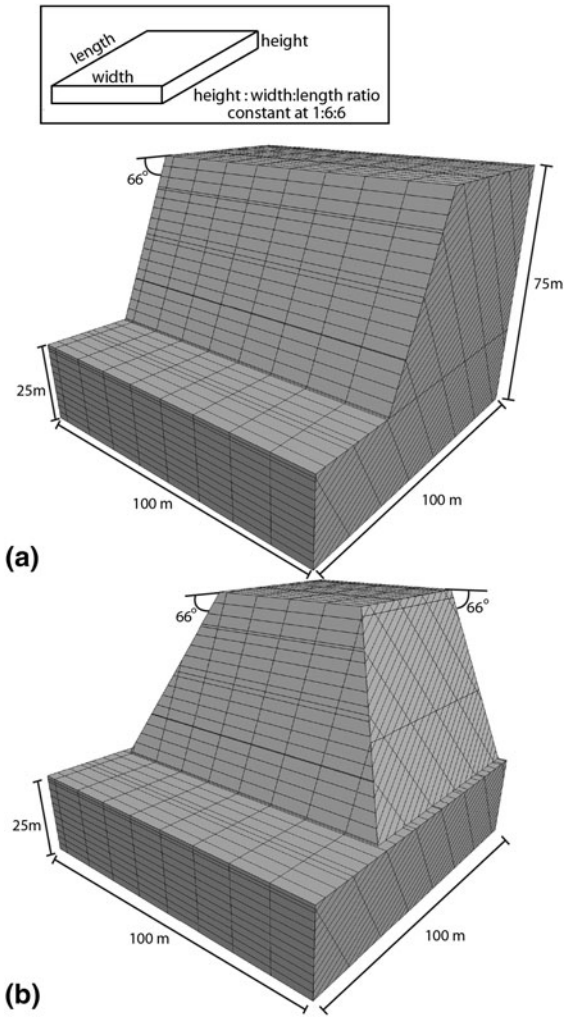

Fig. 1 **a** Geometry of the 3DEC models with assumed vertical and fixed lateral boundaries, **b** geometry of the 3DEC models with assumed sloping and free lateral boundary

3 Results

3.1 Effect of Confinement on the Three-Dimensional Models

Figure 3 compares results from the two 3DEC lateral boundary conditions (model 1 and 2) introduced in Fig. 1 to assess the role of kinematic confinement in three-dimensional translational failure. Figure 3 demonstrates that model 2 sloping and free boundaries (Fig. 3c, d) resulted in a maximum calculated displacement one order of magnitude greater than model 1 with their assumed vertical and fixed lateral boundaries (Fig. 3a, b). While the magnitude of the displacement was different, the movement type in the rock mass ($2 \times 12 \times 12$ m) (Fig. 3) for both lateral boundary conditions (assumed vertical and fixed, sloping and free) involved toe sliding with toppling movement in the slope crest area.

3.2 Influence of the Orientation of the Rear Release Surface

Similar failure mechanisms were obtained in equivalent three-dimensional geometry models with assumed vertical and fixed (Figs. 3a, b; 4a, c) and sloping and free (Figs. 3c, d; 4b, d) lateral boundaries. The observed failure mechanisms ranged from slide-topple (Fig. 3), to simple planar sliding (Fig. 4a, b), and bi-planar (Fig. 4c, d). As mentioned in Sect. 3.1 the calculated displacement values for the model 1 geometries was one order of magnitude smaller than model 2. Table 2 demonstrates that the calculated maximum displacement and volume of the unstable masses (arbitrarily defined as the volume of blocks with displacement greater than 0.1 m after 10,000 numerical time steps) varies as a function of the dip angle of the rear release surface. In both assumed lateral boundary conditions, the greatest unstable volume was obtained when the dip angle of the rear release discontinuity set was 90° (vertical) (Fig. 4a, b). The model 1 series were stable (Table 2; no blocks with displacement greater than 0.1 m after 10,000 numerical steps) for dip angle values of 70° and 80° of the rear release surface (with dip direction of 090°). The minimum unstable volume in the sloping and free models was obtained when the dip angle of the rear release discontinuity sets was 70° (with dip direction of 270°).

When the dip direction of the rear release discontinuity set was varied in the models with assumed vertical and fixed lateral boundaries, asymmetrical slope failures were simulated (Fig. 5a). The higher calculated block displacements were found in the northern end of the slope crest (Fig. 5a). The cross-section suggests the presence of a step-path displacement contour pattern along which the blocks were sliding (Fig. 5a). Variation in the dip direction of the rear release discontinuity set also produced asymmetrical slope failures in the models with assumed sloping and free lateral boundaries, but with higher calculated block displacements in this case indicated at the

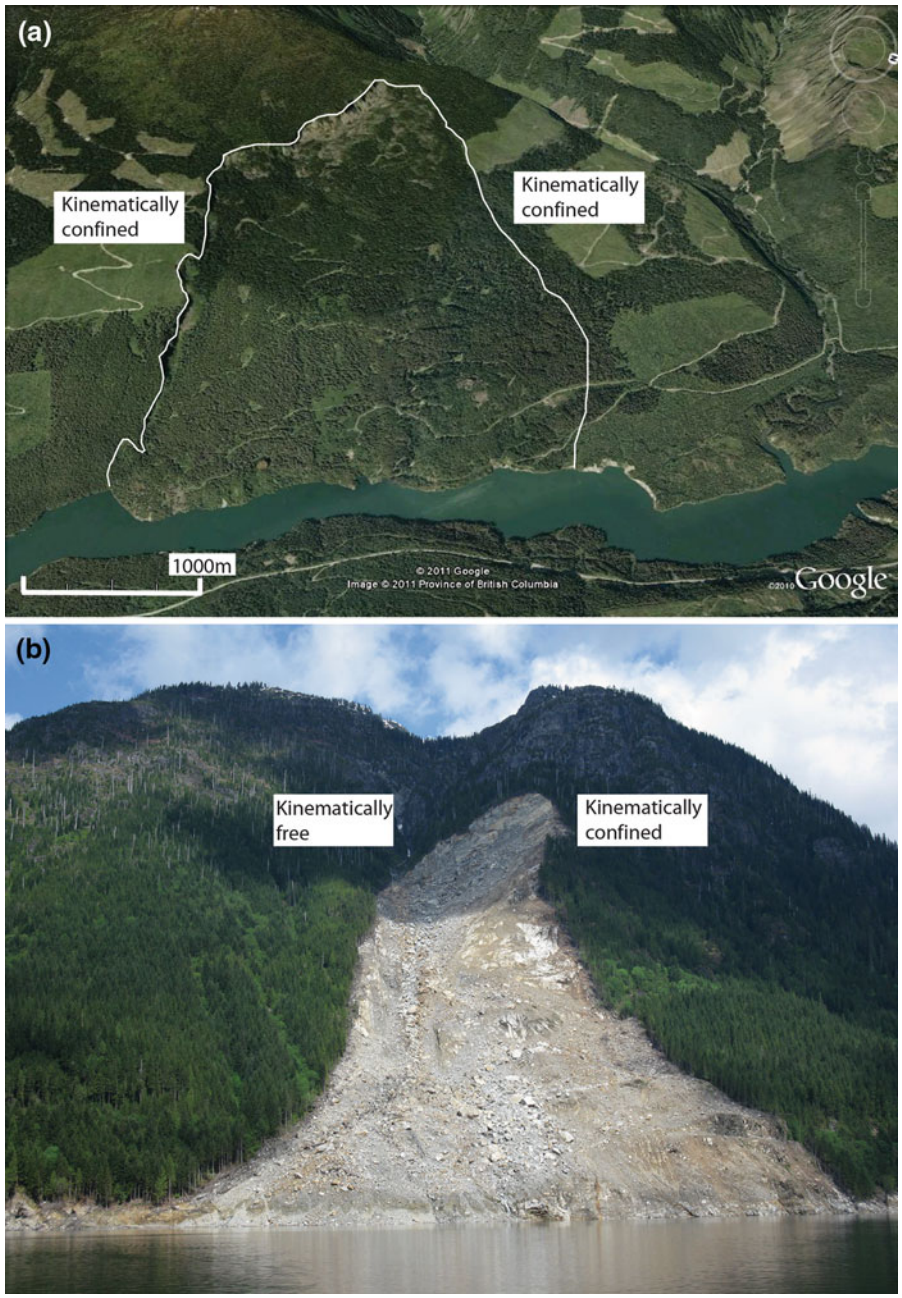

Fig. 2 Example of lateral kinematic confinement in natural rock slopes. **a** The Downie slide (British Columbia, Canada) is kinematically confined along both of its sidescarps (2003 Imagery from Google Earth). **b** The presence of a gully at the Chehalis Lake Landslide (British Columbia, Canada) provides kinematic freedom along one of the sidescarps

southern end of the slope crest (Fig. 5b).The maximum calculated displacement and unstable rock mass volume (sum of block volume with displacement >0.1 m after 10,000 numerical steps) decreased as the dip direction of the rear release changed from 080°, to 070°, to 060° (Table 2). The failure mechanism in the sloping and free models suggests that there is a large region of toe sliding with a weakly toppling column behind it, followed by a second sliding mass (Fig. 5b).

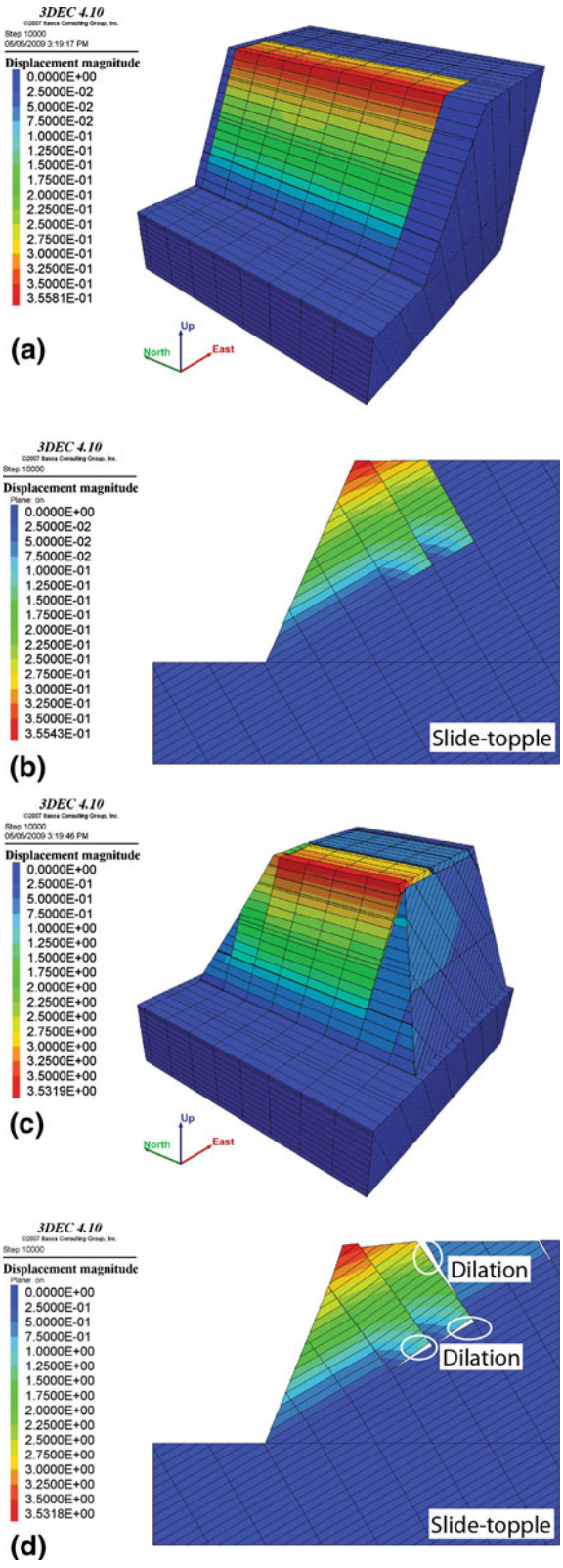

◀ **Fig. 3** Calculated displacement contours in 3DEC (2 × 12 × 12 m block size) with basal discontinuity set 270°/30° (dip direction/dip), and lateral 000°/90°. Rear release discontinuity set of 090°/60° for the assumed **a** vertical and fixed lateral boundary model, **b** longitudinal cross section of the assumed vertical and fixed lateral boundary model, **c** sloping and free lateral boundary model, **d** longitudinal cross-section of the assumed sloping and free lateral boundary model

3.3 Influence of the Dip Direction of the Basal Surface Discontinuity Set

A series of models with assumed vertical and fixed lateral boundary conditions and the dip direction of the basal surface varying between 260° and 240° resulted in stable slope conditions (maximum calculated displacement of less than 0.1 m after 10,000 numerical steps) (Fig. 6a, c; Table 2). In contrast the series of models assuming sloping and free lateral boundary conditions with dip direction of the basal surfaces between 260 and 240° indicated slope failure (Fig. 6b, d). The maximum calculated displacement and failure volume decreased as the dip direction departed from its orthogonal 270° value (Table 2). The cross-section of the model with a 260° dip direction for the basal discontinuity indicates a slide-topple failure mechanism whereas for dip direction values of 250° and 240° the failure mechanism appears to be planar sliding. The displacement contours along the cross-section have a stepped appearance along the basal discontinuity. The overall shape of the unstable volume forms a wedge-like sliding tetrahedron (Fig. 6b, d).

3.4 Influence of the Lateral Release Discontinuity Set Orientation

As the dip direction of the lateral release discontinuity set was varied in the models with assumed vertical and fixed lateral boundary conditions from 010°, to 020°, and 030°, an asymmetric slide-topple slope failure was produced (Fig. 7a) and transitioned into a small volume asymmetric planar sliding slope failure (Table 2 and Fig. 7c). The higher calculated displacement values were observed at the northern end of the model. This was attributed to the dip direction of the lateral release discontinuity being oriented north-northeasterly (010°, 020°, 030°). Should the dip direction of the lateral release discontinuity set have been south-southeasterly (170°, 160°, 150°) the zone

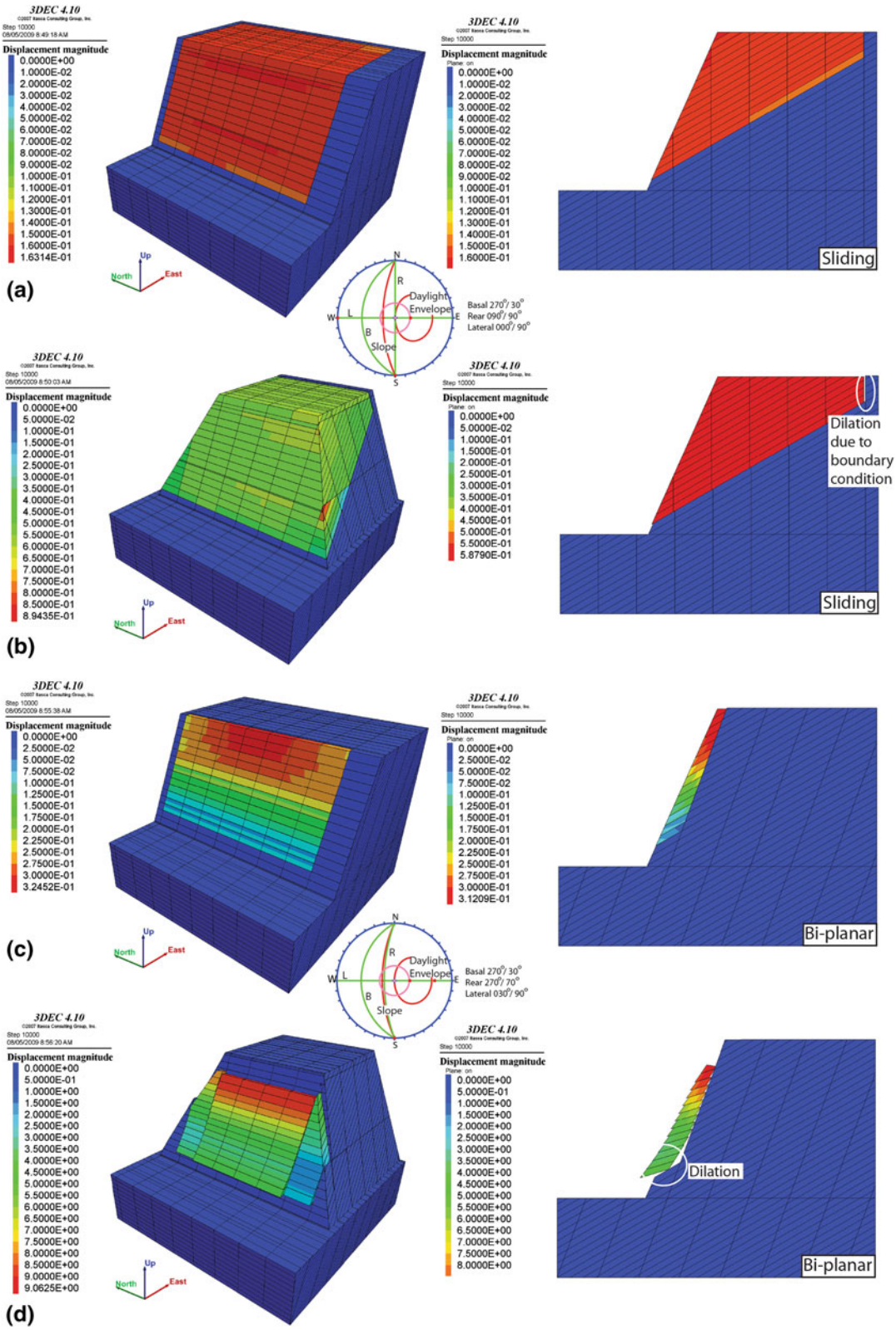
3DEC 4.10
Displacement magnitude
0.0000E+00
1.0000E-02
2.0000E-02
3.0000E-02
4.0000E-02
5.0000E-02
6.0000E-02
7.0000E-02
8.0000E-02
9.0000E-02
1.0000E-01
1.1000E-01
1.2000E-01
1.3000E-01
1.4000E-01
1.5000E-01
1.6000E-01
1.6314E-01
Up
North
East
(a)
N
R
Daylight
Envelope
W
L
E
B
Slope
S
Basal 270/ 30
Rear 090/ 90
Lateral 000/ 90
Sliding
3DEC 4.10
Displacement magnitude
0.0000E+00
5.0000E-02
1.0000E-01
1.5000E-01
2.0000E-01
2.5000E-01
3.0000E-01
3.5000E-01
4.0000E-01
4.5000E-01
5.0000E-01
5.5000E-01
6.0000E-01
6.5000E-01
7.0000E-01
7.5000E-01
8.0000E-01
8.5000E-01
8.9435E-01
5.8790E-01
(b)
Dilation due to boundary condition
Sliding
3DEC 4.10
Displacement magnitude
0.0000E+00
2.5000E-02
5.0000E-02
7.5000E-02
1.0000E-01
1.2500E-01
1.5000E-01
1.7500E-01
2.0000E-01
2.2500E-01
2.5000E-01
2.7500E-01
3.0000E-01
3.2452E-01
3.1209E-01
(c)
Basal 270/ 30
Rear 270/ 70
Lateral 030/ 90
Bi-planar
3DEC 4.10
Displacement magnitude
0.0000E+00
5.0000E-01
1.0000E+00
1.5000E+00
2.0000E+00
2.5000E+00
3.0000E+00
3.5000E+00
4.0000E+00
4.5000E+00
5.0000E+00
5.5000E+00
6.0000E+00
6.5000E+00
7.0000E+00
7.5000E+00
8.0000E+00
8.5000E+00
9.0000E+00
9.0625E+00
8.0000E+00
(d)
Dilation
Bi-planar

◀ **Fig. 4** Calculated displacement contours in 3DEC (2 × 12 × 12 m block size) with basal discontinuity set 270°/30° (dip direction/dip), and lateral 000°/90°. Rear release discontinuity set of 090°/90° for the assumed **a** vertical and fixed, **b** sloping and free lateral boundaries and for rear release discontinuity set of 270°/70° for the assumed, **c** vertical and fixed, **d** sloping and free lateral boundaries

of higher calculated displacement values would have been found at the southern edge of the model.

As the dip angle of the lateral release discontinuity set was varied for the models with assumed vertical and fixed lateral boundary conditions from 80°, to 70° and 60°, the volume of unstable mass (calculated displacement greater than 0.1 m after 10,000 numerical steps) increased. The failure mechanism for all three geometries was planar sliding with the highest calculated displacement concentrated at the northern end of the model for reasons stated previously.

In the series of models with assumed sloping and free lateral boundary conditions, all geometries where the dip direction of the lateral release discontinuity set was varied (010°, 020°, and 030°) led to slide-topple slope failures (Table 2 and Fig. 7b, d). The maximum calculated displacement and volume of the unstable mass decreased progressively as the dip direction was varied from 010°, to 020°, to 030° (Table 2). When the dip angle of the lateral release discontinuity set was varied to 80° and 70° in the models with assumed sloping and free lateral boundaries, it led to slide-topple slope failures with similar maximum calculated displacement and unstable mass volume (Table 2). For the dip angle value of 60°, the main failure mechanism observed consisted of a slide-topple slope failure in the main (eastern) slope face while in the northern lateral boundary a smaller volume of unstable rock mass had a failure mechanism dominated by planar sliding and a secondary rotational component in that plane of failure (Fig. 8). This transition between the two directions of failure movement occurred because the lateral release discontinuity with a dip angle of 60° can act as a planar sliding surface on a slope with a gradient of 66°.

3.5 Influence of the Assumed Block Size

Three-dimensional models where block size was varied led to larger calculated displacements assuming smaller block sizes in the models with assumed sloping and free boundary conditions, but resulted in the opposite behaviour in the models with vertical and fixed boundaries (Table 3 and Fig. 9). For the medium (2 × 12 × 12 m; Fig. 9b) and large blocks (3 × 18 × 18 m; Fig. 9a), the failure mechanism appears to be the same for both lateral boundary conditions (Table 3). The 3DEC models using small blocks (1 × 6 × 6 m; Fig. 9c), predict different failure modes for the different lateral boundary conditions (sliding for the assumed vertical and fixed; toppling for the sloping and free). Table 3 suggests that block size has an influence on the failure mechanism in three-dimensional numerical models.

3.6 Influence of the Discontinuity Persistence

In 3DEC the persistence of discontinuity sets is defined as a probability "p" that any given block that is in the plane of a discontinuity set will be split (e.g. for $p = 1$ all blocks lying in the path of the discontinuity will be split, for $p = 0.25$, 25 % of blocks are split; Itasca 2008). In this project, the effect of persistence was investigated in three stages for the two lateral boundary conditions (Table 4). In the first model only the rear release surface was limited to $p = 0.75$, in the second model the rear and lateral release surfaces were limited to $p = 0.75$, while in the third model all three discontinuity sets were limited to $p = 0.75$. In the models with the vertical and fixed lateral boundary conditions, all three limited persistence scenarios led to stable or marginally stable conditions (0.1 m maximum displacement after 10,000 numerical steps) (Table 4). In the free and sloping boundary condition models, the calculated maximum displacement decreased as the number of discontinuity sets with limited persistence increased (Table 4, Fig. 10). The failure mechanism was also observed to be transitional from a well defined slide-topple for 1 and 2 discontinuity sets with limited persistence (Fig. 10a, b) to sliding dominated when the 3 discontinuity sets had limited persistence (Fig. 10c).

3.7 Influence of the Normal and Shear Stiffness Along Discontinuities

All models investigated in this study assumed a normal and shear stiffness of 5 and 1 GPa/m, respectively. While these values fall within the range of experimental test results previously reported in the

Table 2 Block shape, maximum calculated displacement, failure mechanism, and volume of unstable mass obtained for the various discontinuity sets geometries investigated in the 3DEC models as a function of the assumed kinematic confinement

Rear release		Basal surface		Lateral release		Block shape[a]		Displacement (m)		Failure mode		Failure volume (m^3)	
Dip	Dip direction	Dip	Dip direction	Dip	Dip direction	Alpha	Beta	Model 1	Model 2	Model 1	Model 2	Model 1	Model 2
30	090	30	270	90	000	2.26	2.95	0.14	1.19	Sliding	Sliding	1.62E+04	9.20E+04
40	090	30	270	90	000	2.15	2.63	0.85	5	Slide-topple	Slide-topple	7.94E+04	8.38E+04
50	090	30	270	90	000	2.07	2.1	0.31	4.3	Slide-topple	Slide-topple	5.38E+04	7.72E+04
60	090	30	270	90	000	2.09	2.02	0.36	3.53	Slide-topple	Slide-topple	7.43E+04	9.54E+04
70	090	30	270	90	000	2.11	2.47	0.03	0.37	Stable	Sliding	0	8.40E+04
80	090	30	270	90	000	2.16	2.63	0.04	0.29	Stable	Sliding	0	7.52E+04
90	090	30	270	90	000	2.25	2.95	0.16	1.43	Sliding	Sliding	1.12E+05	1.07E+05
80	270	30	270	90	000	2.58	4.3	0.18	0.57	Sliding	Sliding	1.01E+05	7.55E+04
70	270	30	270	90	000	2.71	4.49	0.32	9.06	Bi-planar	Bi-planar	1.25E+04	1.41E+04
60	270	30	270	90	000	3.23	5.91	0.5	8.89	Bi-planar	Bi-planar	1.45E+04	1.76E+04
60	**080**	30	270	90	000	2.11	2.12	0.36	2.48	Slide-wedge	Slide-topple	2.81E+03	7.48E+04
60	**070**	30	270	90	000	2.17	2.43	0.95	1.48	Sliding	Sliding	7.66E+04	6.46E+04
60	**060**	30	270	90	000	2.29	2.95	0.71	1.19	Sliding	Sliding	7.87E+04	6.45E+04
60	090	30	**260**	90	000	2.09	2.01	0.01	2.38	Stable	Slide-topple	0	7.45E+04
60	090	30	**250**	90	000	2.11	2.07	0.01	1.03	Stable	Sliding	0	5.30E+04
60	090	30	**240**	90	000	2.13	2.51	0.01	0.82	Stable	Sliding	0	4.76E+04
60	090	30	270	**80**	000	2.12	2.11	0.18	3.33	Sliding	Slide-topple	1.37E+03	9.61E+04
60	090	30	270	**70**	000	2.17	2.72	0.67	3.27	Sliding	Slide-topple	8.78E+03	9.61E+04
60	090	30	270	**60**	000	2.29	3.16	0.4	3.03	Sliding	Slide-topple	1.60E+04	9.27E+04
60	090	30	270	90	**010**	2.17	2.12	2.13	4.62	Slide-topple	Slide-topple	6.23E+04	1.04E+05
60	090	30	270	90	**020**	2.19	2.52	2.74	3.38	Slide-topple	Slide-topple	7.69E+04	9.55E+04
60	090	30	270	90	**030**	2.34	3.3	0.6	3.27	Slide	Slide-topple	3.74E+03	9.11E+04

Stability conditions and calculated values refer to model state after 10,000 numerical time steps. Quantities varied in each model run is presented in bold font

[a] Classification scheme after Kalenchuk et al. 2006

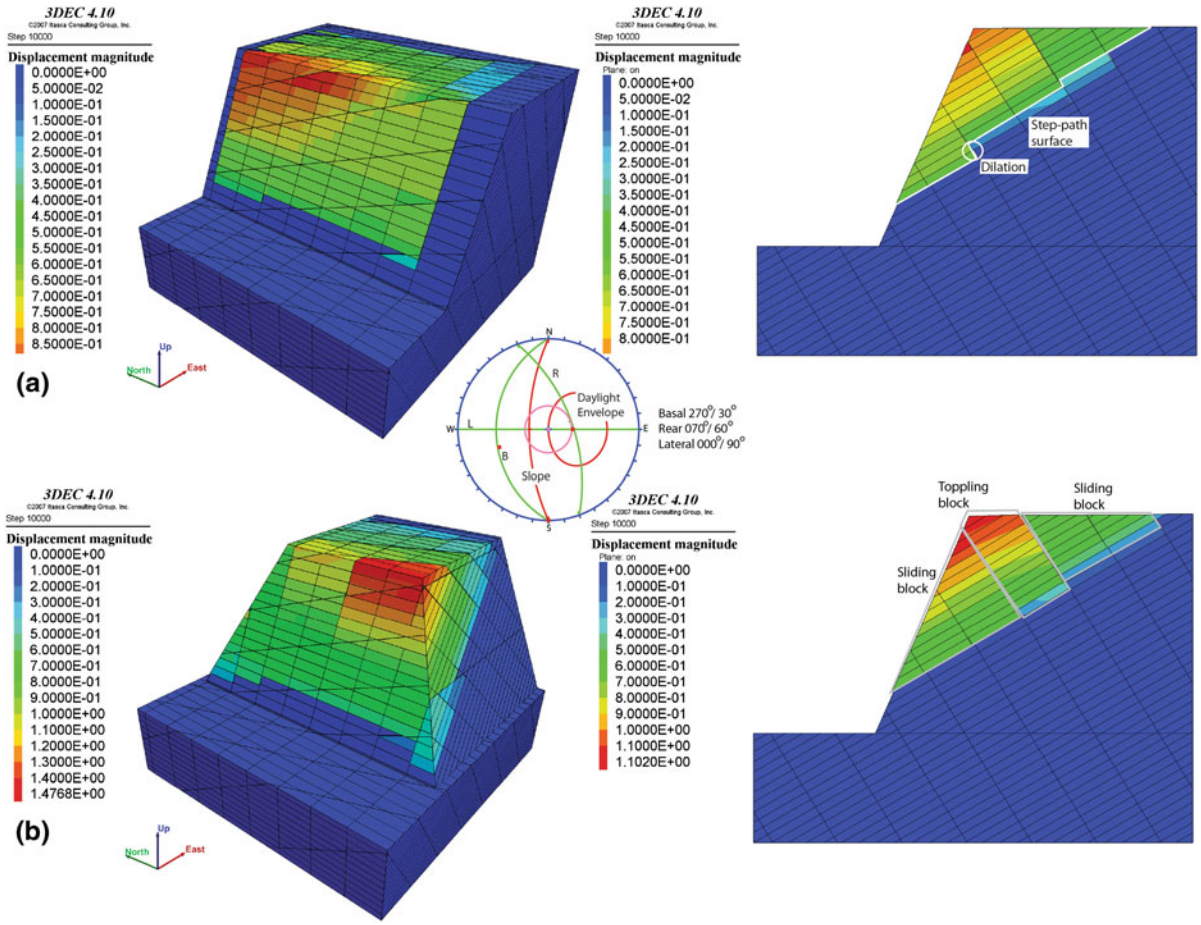

Fig. 5 Calculated displacement contours in 3DEC (2 × 12 × 12 m block size) with rear release discontinuity 070°/60° (dip direction/dip), basal 270°/30°, and lateral 000°/90°. **a** assumed vertical and fixed lateral boundaries, **b** assumed free and sloping lateral boundaries

literature (Kulhawy 1975; Rosso 1976; Bandis et al. 1983) there is always a degree of uncertainty regarding the appropriate values to be used when modelling a natural slope. Several values and ratio of normal and shear stiffness were investigated using the 3DEC reference discontinuity set geometry presented in this paper to assess their influence on the slope stability conditions (Table 5). The results demonstrate that even small changes in stiffness values can significantly affect the values of calculated maximum total displacement and unstable volume. As expected the lower stiffness values (which would correspond to more weathered discontinuity surfaces) resulted in larger values of displacement and unstable volume (Table 5).

4 Discussion

4.1 Failure Mechanisms

The block aspect ratio (height to length to width) 1:6:6 used in this paper was selected to facilitate a planar sliding failure mechanism, however the results presented demonstrate that a slide-topple mechanism can occur in three- dimensional numerical models of a rock mass even where individual blocks have a tabular shape. The development of the slide-topple mechanism is attributed to the fully persistent nature of the rear release (toppling) discontinuity set which can act as a single column when the rock mass is confined and/or the block size is small enough relative to the size of

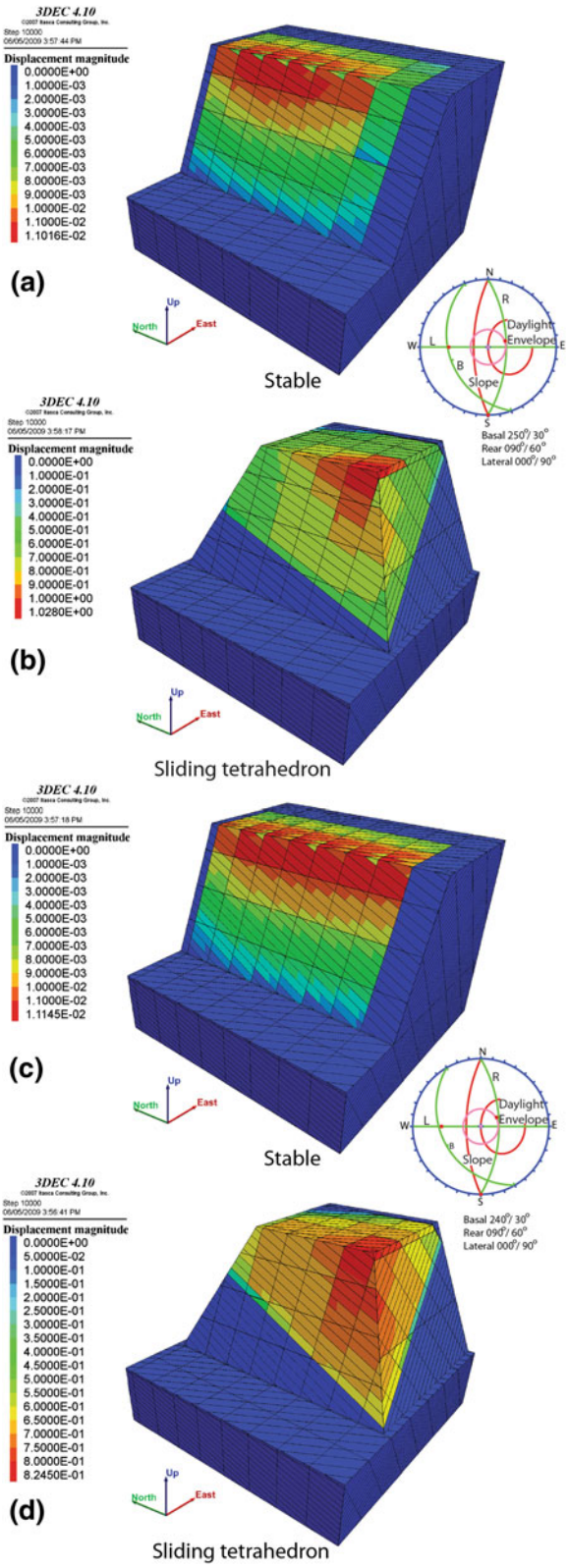

◀ **Fig. 6** Calculated displacement contours in 3DEC (2 × 12 × 12 m block size) with lateral discontinuity set 000°/90° (dip direction/dip) and rear release discontinuity set of 090°/60° and a basal discontinuity of 250°/30° with assumed **a** vertical and fixed, **b** sloping and free lateral boundaries and for basal discontinuity set of 240°/30° with an assumed, **c** vertical and fixed, **d** sloping and free lateral boundaries

the slope. This phenomenon had previously been described by Aydan et al. (1989) for base friction physical models with fully persistent discontinuities. These findings therefore suggest that classification schemes such as proposed by Ashby (1971) and toppling nomograms (Choquet and Tanon 1985) should only be applied when investigating the stability of an individual rock block, a rock mass with discontinuities of limited persistence relative to the size of the slope of interest or where the blocks in the rock mass are relatively large compared to the slope of interest.

In the numerical models where sliding and toppling both occurred (e.g. Figs. 3b, d, 5, 7a, b, d, 8b, 10a, b), the sliding occurred in the lower portion of the model while toppling occurred in the upper portion of the slope. These results are consistent with the limit equilibrium solution proposed by Goodman and Bray (1976) and could be classified as slide head toppling according to the mass movement classification proposed by Goodman and Kieffer (2000). This mode of failure is regarded as a secondary toppling that occurs due to the "new" space created by the sliding block. In the models investigated in this paper, the over-steepened toe needed for toppling to develop, as discussed by Nichol et al. (2002), was created by the sliding toe block. The bi-planar failures presented in Fig. 4c, d have a backward rotational component to them. This corresponds to a block slumping rock slope failure mechanism as described by Kieffer (2003, 2006) and Kinakin (2004). The unstable rock mass in the two-dimensional bi-planar failure models has a smaller area and different shape (columnar) than the sliding or slide-topple models. The slopes where a bi-planar failure mechanism is present also exhibit the

Fig. 7 Calculated displacement contours in 3DEC (2 ×▶ 12 × 12 m block size) with basal discontinuity set 270°/30° (dip direction/dip), rear release discontinuity set of 090°/60° and a lateral release discontinuity of 020°/90° with assumed **a** vertical and fixed, **b** sloping and free lateral boundaries and for a lateral release discontinuity set of 030°/90° with assumed, **c** vertical and fixed, **d** sloping and free lateral boundaries

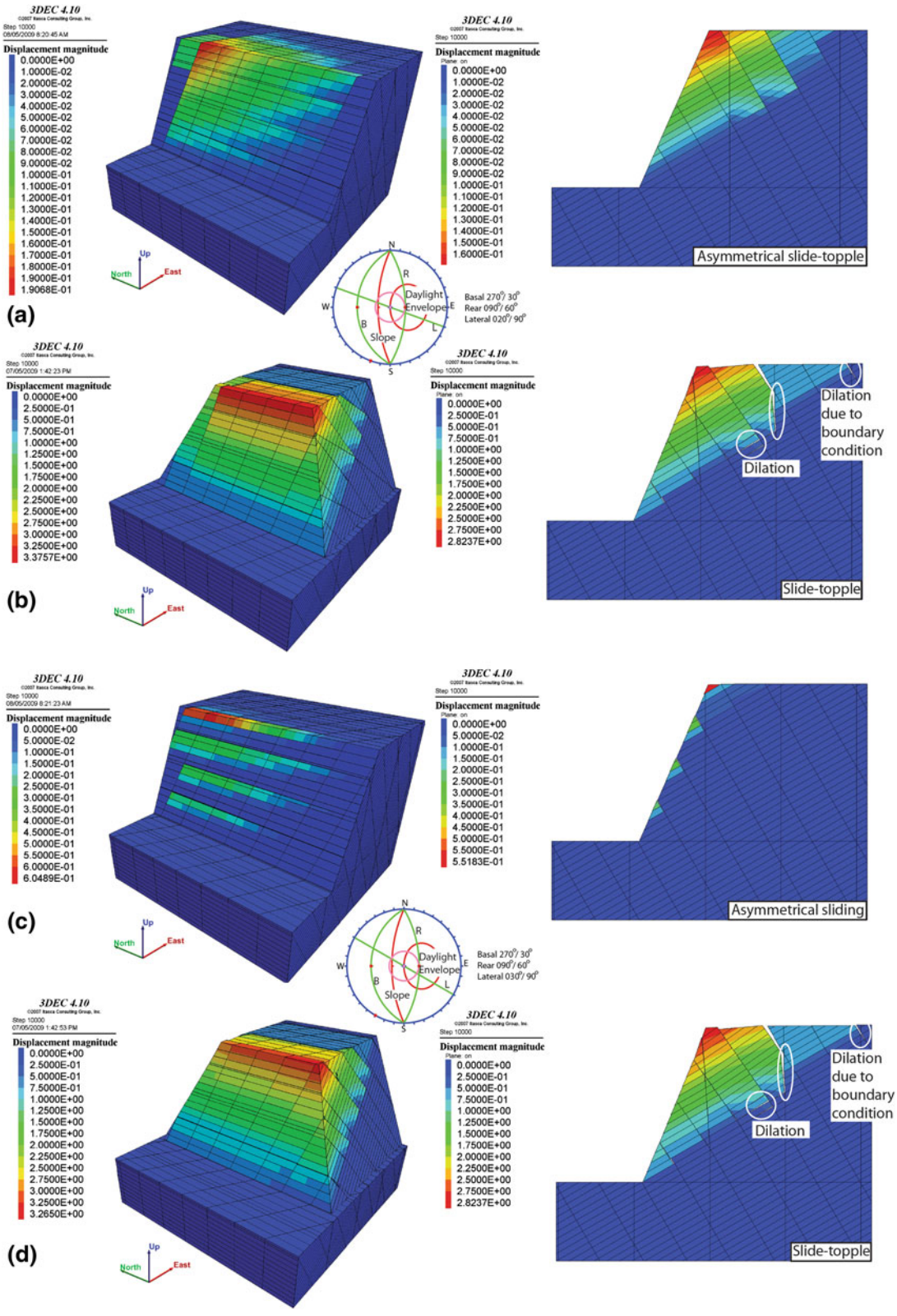
3DEC 4.10
Displacement magnitude
0.0000E+00
1.0000E-02
2.0000E-02
3.0000E-02
4.0000E-02
5.0000E-02
6.0000E-02
7.0000E-02
8.0000E-02
9.0000E-02
1.0000E-01
1.1000E-01
1.2000E-01
1.3000E-01
1.4000E-01
1.5000E-01
1.6000E-01
1.7000E-01
1.8000E-01
1.9000E-01
1.9068E-01
Up
North
East
(a)
N
R
Daylight Envelope
E
W
B
L
Slope
S
Basal 270°/ 30°
Rear 090°/ 60°
Lateral 020°/ 90°
Asymmetrical slide-topple
(b)
2.5000E-01
5.0000E-01
7.5000E-01
1.0000E+00
1.2500E+00
1.5000E+00
1.7500E+00
2.0000E+00
2.2500E+00
2.5000E+00
2.7500E+00
3.0000E+00
3.2500E+00
3.3757E+00
2.8237E+00
Dilation due to boundary condition
Dilation
Slide-topple
(c)
5.0000E-02
5.5183E-01
Basal 270°/ 30°
Rear 090°/ 60°
Lateral 030°/ 90°
Asymmetrical sliding
(d)
3.2650E+00
Dilation due to boundary condition
Dilation
Slide-topple

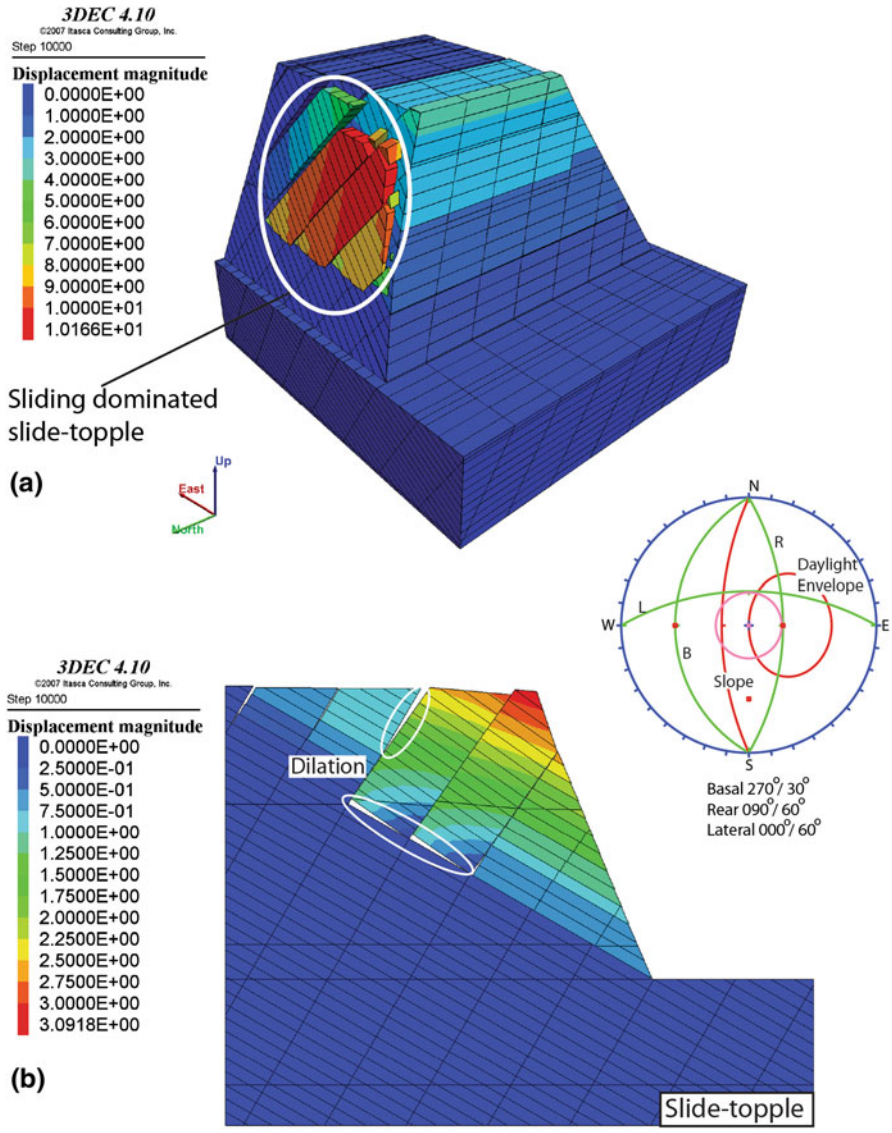

Fig. 8 Calculated displacement contours in 3DEC (2 × 12 × 12 m block size) with basal discontinuity set 270°/30° (dip direction/dip), rear release discontinuity set of 090°/60° and a lateral release discontinuity of 000°/60°. Note that in **a** a small volume of the rock mass is failing by a planar sliding failure mechanism. **b** Cross-section highlighting that the main volume of the rock mass is failing via a slide-topple mechanism

Table 3 Maximum calculated displacement and dominant failure mechanism obtained in the 3DEC models as a function of block size and degree of kinematic confinement

Block size (HxLxW m)	Lateral boundaries	Displacement (m)	Failure mode
1 × 6 × 6	Vertical and fixed	0.11	Sliding
2 × 12 × 12	Vertical and fixed	0.36	Slide-topple
3 × 18 × 18	Vertical and fixed	0.42	Sliding
1 × 6 × 6	Sloping and free	6.05	Topple
2 × 12 × 12	Sloping and free	3.53	Slide-topple
3 × 18 × 18	Sloping and free	0.84	Sliding

smallest unstable volume in the three-dimensional models with assumed sloping and free lateral boundaries. In the model where the dip direction of the basal surface was varied for the free and sloping boundary conditions (Fig. 6b, d) the sliding tetrahedron rock mass corresponds to the type-two failure based on the classification by Yoon et al. (2002) for sliding blocks for a multi-faced slope.

Table 4 Maximum calculated displacement and dominant failure mechanism obtained in the 3DEC models as a function of the discontinuity set persistence

Assumed persistence in 3DEC	Lateral boundaries	Displacement (m)	Failure mode
$p = 0.75$ on RR $p = 1$ on LR and BS	Vertical and fixed	0.01	Stable
$p = 0.75$ on RR and LR $p = 1$ on BS	Vertical and fixed	0.10	Minor sliding
$p = 0.75$ on RR, LR, and BS	Vertical and fixed	0.04	Stable
$p = 0.75$ on RR $p = 1$ on LR and BS	Sloping and free	1.81	Slide-topple
$p = 0.75$ on RR and LR $p = 1$ on BS	Sloping and free	1.54	Slide-topple
$p = 0.75$ on RR, LR, and BS	Sloping and free	0.60	Sliding

RR rear release, *LR* lateral release, *BS* basal surface

Table 5 Maximum calculated displacement and volume of unstable mass obtained after 10,000 numerical time steps for different values of normal and shear stiffness along the discontinuities

Lateral boundaries	Kn (GPa/m)	Ks (GPa/m)	Displacement (m)	Failed volume (m^3)
Vertical and fixed	10	2	0.06	Stable
Vertical and fixed	10	1	0.07	Stable
Vertical and fixed	5	5	0.14	2.19E+03
Vertical and fixed	5	1	0.36	7.34E+04
Vertical and fixed	1	0.2	1.56	9.60E+04
Sloping and free	10	2	2.99	8.99E+04
Sloping and free	10	1	3.08	9.19E+04
Sloping and free	5	5	6.05	9.14E+04
Sloping and free	5	1	3.53	9.54E+04
Sloping and free	1	0.2	32.62	9.65E+04

4.2 Block Size

Using the two-dimensional distinct element code UDEC, Hencher et al. (1996) investigated the influence of block size on slope rock mass behaviour. They reported higher maximum displacement values for larger blocks. A study by Corkum and Martin (2004) using 3DEC obtained higher displacement and volumetric dilation values as the number of blocks in their models was increased (i.e. smaller blocks). In the results presented in Table 3, a similar finding (smaller blocks leading to larger displacement) was obtained for the models with an assumed sloping and free lateral boundary. The different influence of the scale effects on the maximum calculated displacement values between the two- and three-dimensional numerical models is emphasized. This is due to the differences in slope and block geometries assumed in this paper and the models of Hencher et al. (1996) and Corkum and Martin (2004) and to the role of kinematic confinement in three-dimensional distinct element models. Further work on this aspect is required to confirm these observations.

Hencher et al. (1996) also demonstrated that the two-dimensional rock slope failure mechanism was influenced by the block size. They found that for blocks with an aspect ratio of 1:1 (square), a planar sliding failure mechanism was simulated in models with smaller blocks while toppling occurred in models with larger blocks. The results presented herein indicate that sliding failure occurs (along a basal plane with a dip of 30° and a friction angle of 29°) when larger block geometries are assumed and that slide-topple dominates in smaller block size models (Table 2). This difference in results is attributed to the tabular block shape (1:6 aspect ratio) used in the models presented in this paper which facilitated the sliding mechanism for larger blocks.

Recently work by Hammah et al. (2009) showed that scale effects in rock slope analysis could also be modelled in a finite element code with explicit representation of joint sets and shear strength

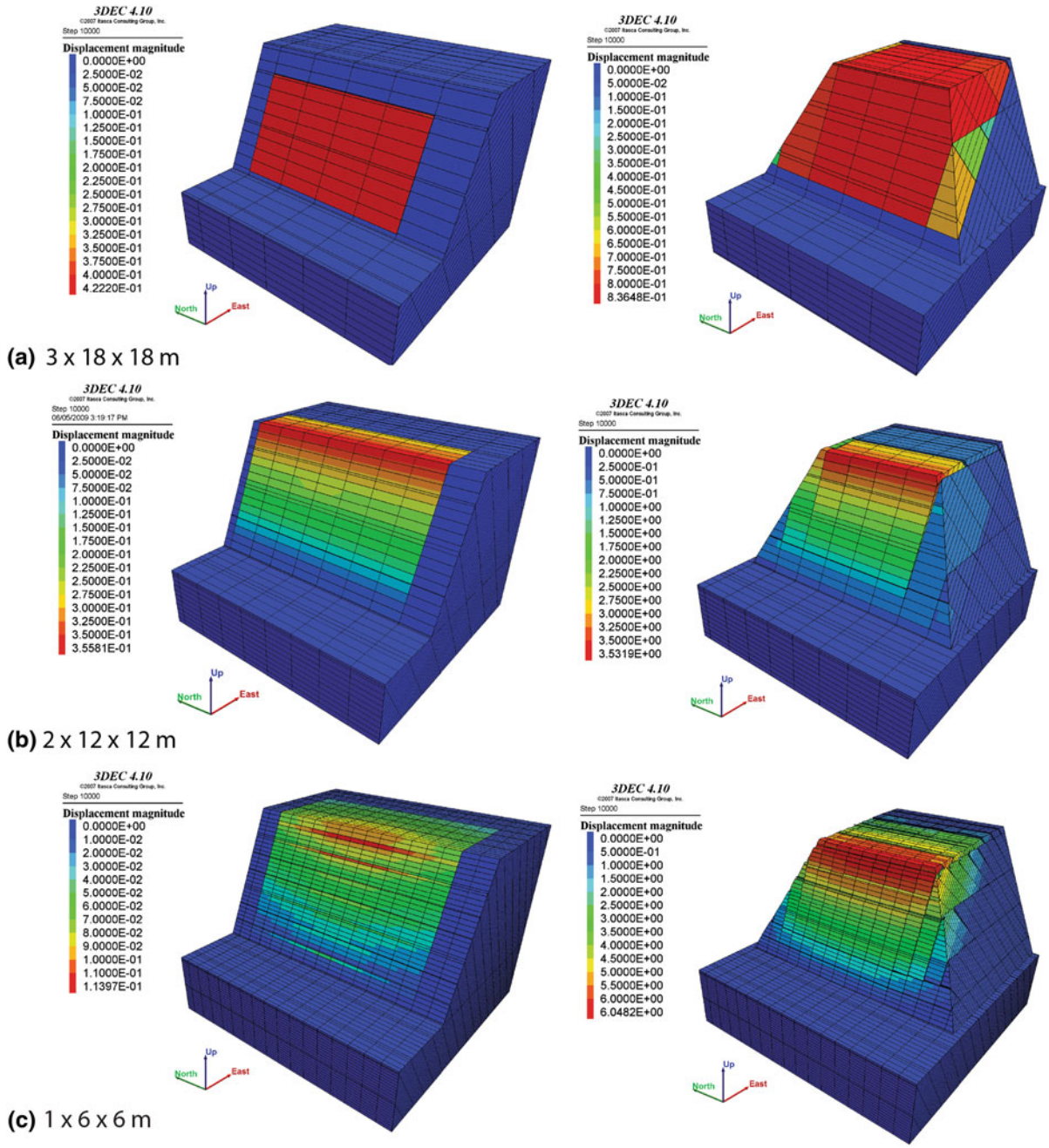

Fig. 9 Calculated displacement contours in 3DEC models with basal discontinuity set 270°/30° (dip direction/dip), rear release discontinuity set of 090°/60° and a lateral release discontinuity of 000°/90°. **a** 3 × 3 × 18 m, **b** 2 × 12 × 12 m, **c** 1 × 1 × 6 m blocks

reduction (SSR) analysis techniques. Their results demonstrated that for large blocks relative to the slope height, simple structurally controlled failure occurred while semi-circular failures developed in numerical models with small block size relative to the slope height. They also reported that the factor of safety (FOS) calculated by the SSR analysis technique decreased with reduction in block size (relative to

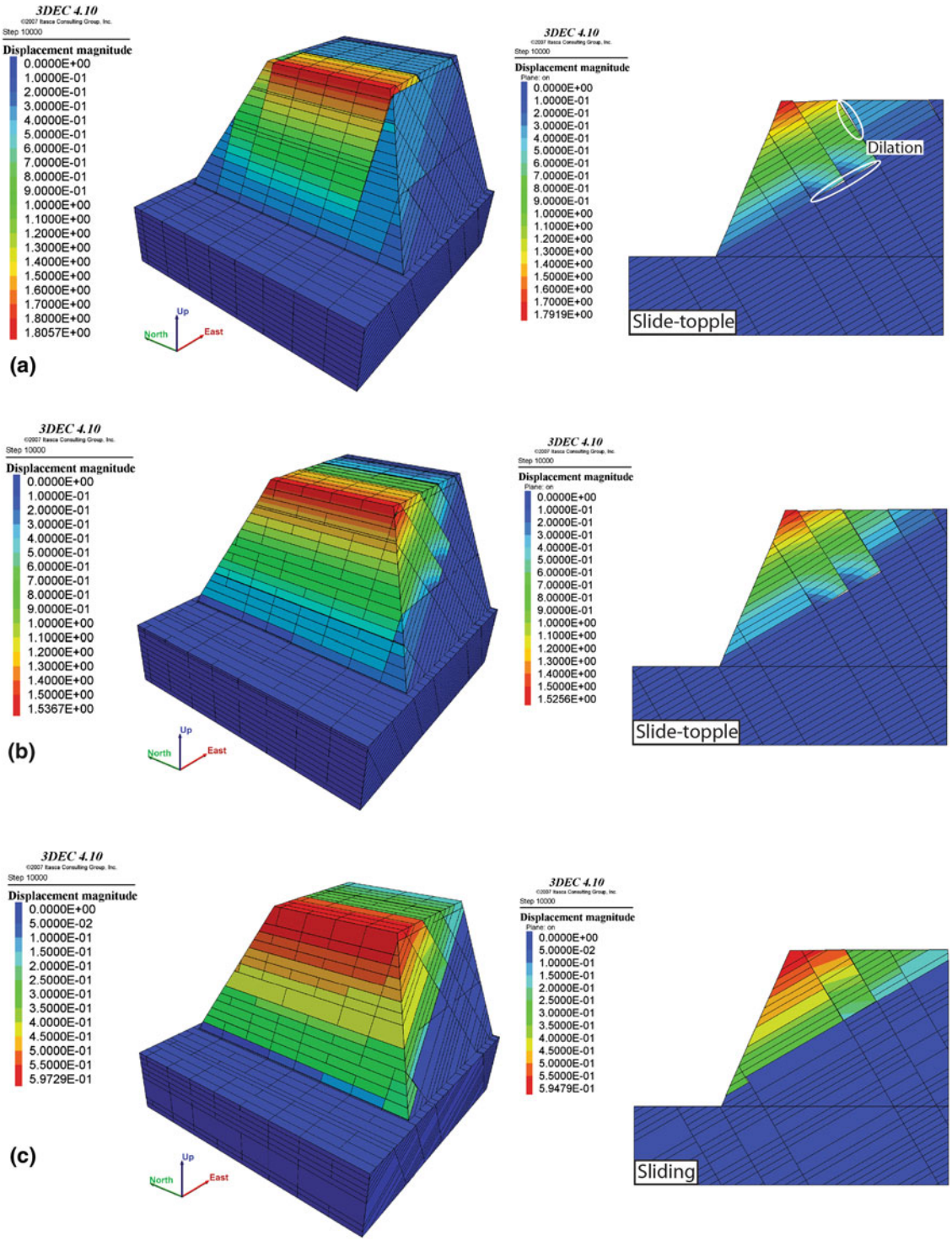

Fig. 10 Calculated displacement contours in 3DEC (2 × 12 × 12 m block size) with basal discontinuity set 270°/30° (dip direction/dip), rear release discontinuity set of 090°/60° and a lateral release discontinuity of 000°/90°. Discontinuity persistence of **a** $p = 0.75$ on RR, $p = 1$ on BS and LR, **b** $p = 0.75$ on RR, and LR; $p = 1$ on BS, **c** $p = 0.75$ on RR, LR, and BS, where *RR* rear release, *LR* lateral release, *BS* basal surface

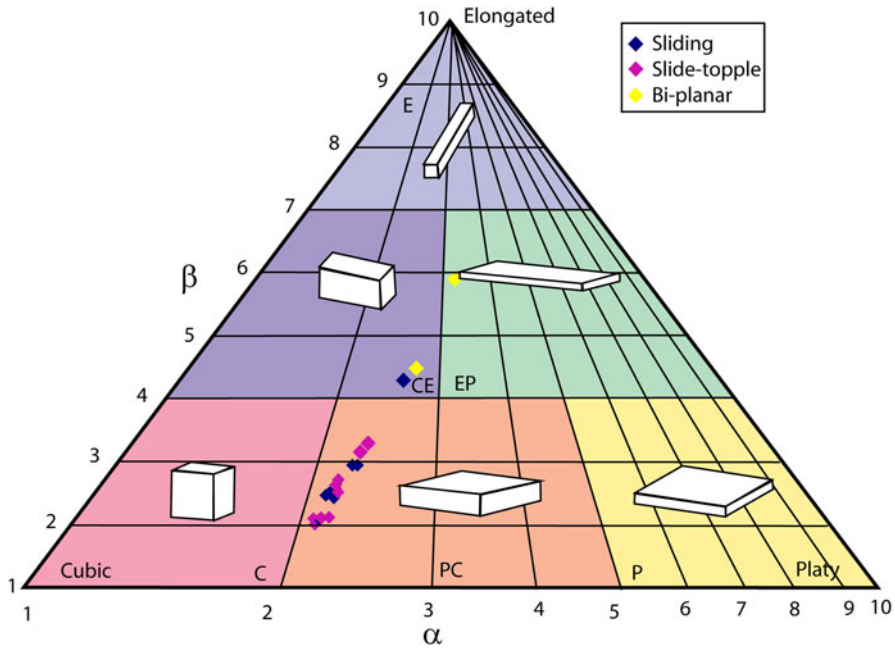

Fig. 11 Block shapes modeled in this paper represented in the classification and block shape diagram proposed by Kalenchuk et al. 2006

the slope height) (Hammah et al. 2009). Similarly, work from Sitar et al. (2005) using the Discontinuous Deformation Analysis (DDA) code to model the Vajont landslide found higher block velocities in models with greater number of blocks. Assuming that the calculated maximum displacement can be used as a proxy for the factor of safety (since the SSR techniques are applied only to deformable material), the results in Table 3 suggest that the lower FOS would be associated with the smaller blocks in the three-dimensional 3DEC models.

4.3 Slope Confinement

Recent work by Galic et al. (2008) has investigated the role of confinement in physical models of sliding blocks on a multi-faceted sliding surface. They confirmed that increased lateral constraint in physical models led to higher effective friction angles. The results presented in Fig. 3 demonstrate that the expected displacement values from a slope with sloping and free lateral conditions can be an order of magnitude greater than for a slope with vertical and fixed lateral condition. Just as in the experiments by Galic et al. (2008) these results are attributed to the dilation that can occur in the slopes (or blocks) with lesser degrees of kinematic confinement. In the models investigated in this paper, a change of ±20° in the dip direction of the basal surface led to increased stability in the models with assumed vertical and fixed lateral boundaries. This corresponds to the value quoted in textbook for the difference between the dip direction of the sliding surface and the orientation of the slope (e.g. Wyllie and Mah 2004). The conditions of assumed vertical and fixed lateral boundaries are thought to represent the geometry present along an open-pit bench, while the assumed sloping and free lateral boundaries would be more representative of a road cut through an isolated topographic high. Both of these situations are therefore feasible and the potential for rock mass dilation (such as in the sloping and free lateral boundaries) should be noted during site investigation and included in the slope stability analysis. Similar results were also obtained by Palassi and Ashitiani (2008) who compared two- and three-dimensional distinct element models (UDEC and 3DEC). They found that the UDEC models had a higher factor of safety than the equivalent three-dimensional convex slope profile.

4.4 Block Shape

The three-dimensional shape of the blocks created by the discontinuity set geometries (basal, rear, and lateral release surfaces) investigated in this paper was characterized using the methodology proposed by

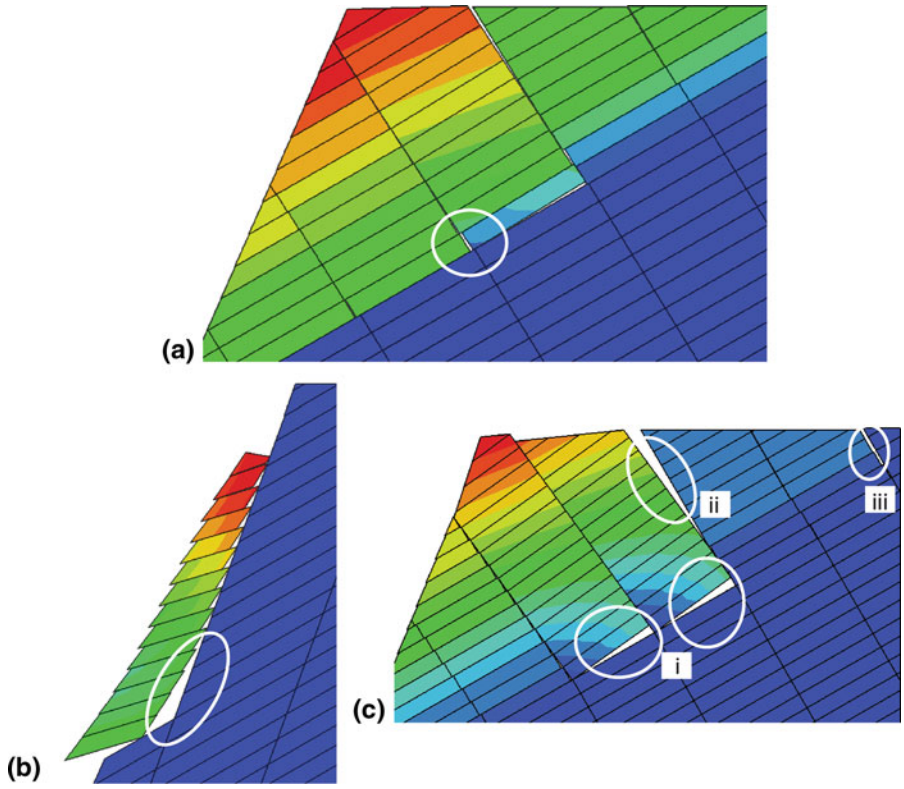

Fig. 12 Dilation observed in the rock masses investigated in this chapter. Dilation associated with **a** planar sliding, **b** bi-planar, **c** toppling (i—along basal surface; ii—along rear release; iii—due to boundary conditions)

Kalenchuk et al. (2006). The alpha (α) parameter is a measure of the shortening of the short axis of the block while the beta (β) parameter is a measure of the elongation of the long axis of the block; both of which were reported in Table 2. The alpha and beta parameters obtained were also summarized in a block shape diagram (Fig. 11). Two blocks fell in the cubic/elongated category and the block created by the geometry (rear, basal, and lateral release) 60°/270° (dip/dip direction), 30°/270°, and 90°/000° fell in the elongated/platy category. The two discontinuity set orientation combinations that resulted in slope failures through a bi-planar mechanism fell within these three outliers. The elongated character of the blocks facilitated the nature of this failure mechanism. The block shape was not found to control the transition between the sliding and slide-topple failure mechanisms. Block size (Sect. 4.2) and the persistence of the discontinuity sets (Sect. 4.6) appear to be more important in the transition between the sliding and slide-topple failure mechanisms.

4.5 Step-Path and Rock Mass Dilation

The development of step-path failure surfaces is generally associated with non-fully persistent discontinuity sets (Jennings 1970; Einstein et al. 1983; Goodman 2003) and it has been observed in laboratory experiments (Bobet and Einstein 1998), numerical models (Eberhardt et al. 2004; Yan et al. 2007a, b; Franz and Cai 2008) and in field studies (Yan 2008; Brideau et al. 2009; Sturzenegge and Stead 2012). The notion of step-path failure surface geometry is also implicit in the analytical solution to block toppling by Goodman and Bray (1976). The results presented in this paper demonstrate that stepped-failure surfaces can also develop in models with fully persistent discontinuity sets. Figures 3b and 10a show the development of a step failure surface along the fully persistent basal discontinuity set. While the step-path failure in non-persistent discontinuities in a rock mass results from stress concentrations and induced intact rock fractures; the step-paths in the models presented

in this paper are due to rock mass dilation and discontinuous displacement along the fully persistent discontinuity sets. In these models, dilation was observed at different locations and associated with different failure mechanisms. Figure 12a demonstrates dilation in the rock mass associated with planar sliding, Fig. 12b demonstrates the A-void associated with the bi-planar failure, while Fig. 12c illustrates the dilation occurring at the base and rear of a toppling column. Dilation associated with boundary conditions is outlined in Fig. 12c iii. Models with extended dimensions were investigated to confirm that the boundary conditions highlighted in Fig. 12c did not affect the depth of the failure surface or the failure mechanism.

4.6 Discontinuity Set Persistence and Shear Strength

The role of limited persistence discontinuities was investigated in base friction physical models by Aydan et al. (1989) who found that limited persistence increased the stability field. The role of the discontinuity set persistence was also investigated by Franz (2009) using 3DEC to model the importance of the lateral and rear release discontinuity sets at the Cadia Hill Open Pit in Australia. He found that the extent of the unstable rock mass was influenced by discontinuity persistence (Franz 2009). In the results presented in this paper, the increased stability field was observed in the 3DEC models with vertical and fixed boundary conditions. A limited persistence of 75 % for even one discontinuity set led to a stable rock mass (Table 4). The limited persistence in the 3DEC model with free and sloping lateral boundaries (Fig. 10) also demonstrated that the failure mechanism can be influenced by the persistence of the discontinuity sets. The focus on the variation in persistence in the models presented in this paper was to demonstrate the important role this factor plays in rock slope stability. A systematic and exhaustive study would investigate the sensitivity of the rock slope stability to the degree of discontinuity persistence (i.e. "*p*" factor in 3DEC), and the permutations of the discontinuity sets of limited persistence (i.e. the order in which the persistence of the discontinuity sets is limited). Finally, a factor not considered in this paper that could also influence the failure mechanisms and volumes of an unstable rock mass is the varied strength (shear and/or tensile) along the different discontinuity sets in a given model. Work by MacLaughlin and Sitar (1996) and Sitar et al. (2005) has demonstrated using a DDA code that a toppling or sliding failure mechanism could be favoured in models with the same geometry but with different friction angles on the discontinuity sets.

4.7 Influence of Mechanical Time Step on Numerical Modelling Results

The mechanical time step is a crucial parameter for obtaining a stable and valid solution in a distinct element code. In 3DEC, it is a function of the deformation of the material (not relevant in this study because the blocks are assumed to be rigid) and the movement along the discontinuities. The limiting time step associated with displacement along the discontinuity is controlled by the discontinuity normal and shear stiffness and the smallest block in the model. The joint normal and shear stiffness are the same in all models with the exception of the series of models where the sensitivity to stiffness was specifically considered (Sect. 3.7 and Table 5). The models where the orientation of the discontinuity sets were varied (Sects. 3.2–3.4 and Table 2) all have very similar smallest block size values. The series of models where the block size (Sect. 3.5 and Table 3) and persistence (Sect. 3.6 and Table 4) were varied resulted in a range of values for the smallest block. Overall the time step for the great majority of models investigated in this study should be the same or very close in value. This is important if the block movements/overall rock slope deformation modes are to be compared between models after a given number of mechanical time steps. Within the limits mentioned above the authors suggest the trend/general behavior of the rock mass deformation has been appropriately captured by the numerical modelling results presented. The absolute values of the displacement and unstable volume are not considered as rigorous estimates but are intended to provide a semi-quantitative means of expressing the difference between the models. Comparison between models with different block sizes and discontinuity stiffness is not a trivial procedure and the results of such comparisons must be treated appropriately. (Section 4.2).

4.8 The Importance of Kinematic Boundary Conditions in Natural Rock Slopes

The rock mass deformation behaviour described in the conceptual slope models investigated in this paper can also be observed in natural rock slopes. The Downie Slide is a 150 Mm^3 slow moving gneissic rock mass on the shore of the Revelstoke hydro-electrical reservoir in British Columbia, Canada. It can be categorised as kinematically confined on both sides (Fig. 2a). 3DEC models by Kalenchuk et al. (2009a) suggest that the dip direction of the rear release surface is not parallel to that of the slope. The difference between the dip direction of the slope and rear release surface has led to the development of the stepped appearance of the sidescarp (as observed in the field by Kalenchuk et al. 2009b). Kalenchuk et al. (2009b) reported on the complex measured displacement pattern and noted that there is a rotational component in plan to the movement. These field conditions are analogous to the conceptual models investigated in this paper where the lateral boundary conditions were assumed to be vertical and fixed and led to asymmetrical displacement patterns when the dip direction of the rear release were varied (Fig. 5).

The Chehalis Lake Landslide is a 3 Mm^3 rock slope failure in granodioritic rocks that occurred in December 2007 along the northwestern shore of Chehalis Lake, in southern British Columbia (Brideau et al. 2011). The slope failure has one kinematically free and one confined lateral boundary (Fig. 2b). The presence of the kinematically free boundary allowed for the development of an unstable rock mass with a basal discontinuity dipping into the gully. This created a sliding tetrahedron similar to the ones presented in Fig. 6b, d. Additional examples of the importance of kinematic boundary conditions and orientation of basal/lateral/rear release discontinuities in natural slopes can be found in Brideau and Stead (2011)

5 Conclusions

The orientation of the rear, basal and lateral release surfaces along with kinematic confinement, block size, and discontinuity set persistence were all shown to influence the calculated displacement, volume, displacement direction, and failure mechanism of an unstable rock mass in three-dimensional distinct element models. The following observations can be made;

- Changes in the orientation of the rear release discontinuity set from 30°/090 (dip/dip direction) to 60°/270 led to transition of the failure mechanism from a slide-topple, to sliding, and to bi-planar in models assuming either vertical/fixed or sloping/free lateral boundaries.
- Changes of ±20° in the dip direction of the rear release discontinuity set led to the development of an asymmetrical unstable rock mass in the models with assumed vertical and fixed lateral boundaries.
- Changes of ±20° in the dip direction of the basal surface led to increased stability in the models with assumed vertical and fixed lateral boundaries.
- Changes of ±20° in the dip direction of the lateral release led to small volumes of unstable rock mass in the models with vertical and fixed lateral boundaries.
- Changes of ±20° in the dip angle of the lateral release discontinuity set led to the development of an asymmetrical rock mass in the models with vertical and fixed lateral boundaries.

The values and direction of the calculated maximum total displacement in the models with sloping and free lateral boundaries were also influenced by variation of the orientation of the rear, basal and lateral release surfaces although their influence on the slope stability and failure mechanism were not as pronounced as in the vertical and free models.

The block size was shown to influence the failure mechanism in the three-dimensional numerical models. Kinematic confinement was found to have a marked influence on the calculated maximum displacement. The persistence of the discontinuity sets in the numerical models was also demonstrated to have an important role on the calculated displacement and dominant failure mechanism. The numerical modelling results using the three-dimensional distinct element code were demonstrated to be sensitive to the assumed values for the normal and shear stiffness along the discontinuity surfaces.

In summary the results presented suggest that the identification of a discontinuity set in a kinematic analysis which leads to a potential planar failure mechanism for a finite and removable block might on its own not be sufficient to assume that planar sliding will be the dominant failure mechanism. A through-

going basal joint set has been shown to result in planar sliding, slide-topple, or bi-planar failures depending on the orientation of the rear release surface, block size, and discontinuity persistence.

Acknowledgments The authors would like to acknowledge funding from NSERC, Simon Fraser University Graduate Scholarship, and the FRBC Resource Geoscience and Geotechnics Endowment Fund. The authors would also like to thank D. vanZeyl for his assistance with the 3DEC plots.

References

Ashby J (1971) Sliding and toppling modes of failure in model and jointed rock slopes, M.Sc. thesis London University, Imperial College, 60 p

Aydan O, Shimizu Y, Ichikawa Y (1989) The effective failure modes and stability of slopes in rock mass with two discontinuity sets. Rock Mech Rock Eng 22:163–188

Bandis SC, Lumsden AC, Barton NR (1983) Fundamentals of rock joint deformation. Int J Rock Mech Min Sci Geomech Abstr 20(6):249–268

Bobet A, Einstein HH (1998) Fracture coalescence in rock-type material under uniaxial and biaxial compression. Int J Rock Mech Min Sci 35(7):863–888

Bray JW, Goodman RE (1981) The theory of base friction models. Int J Rock Mech Min Sci Geomech Abstr 18: 453–468

Brideau M-A, Stead D (2009) The role of rear release surfaces, block size and lateral confinement on rock slope failure mechanisms. In: 62nd Canadian geotechnical conference and 10th joint groundwater CGS/IAH-CNC conference. Halifax, Nova Scotia, pp 489–496

Brideau M-A, Stead D (2010) Controls on block toppling using a 3-dimensional distinct element approach. Rock Mech Rock Eng 43(3):241–260

Brideau M-A, Stead D (2011) The influence of three-dimensional kinematic controls on rock slope stability. In: Sainsbury D, Hart R, Detournay C, Nelson M (eds) Proceedings of the 2nd international FLAC/DEM symposium, Melbourne, Australia, February 2011, pp 213–220

Brideau M-A, Yan M, Stead D (2009) The role of tectonic damage and brittle rock fracture in the development of large rock slope failures. Geomorphology 103(1):30–49

Brideau M-A, Sturzenegger M, Stead D, Jaboyedoff M, Lawrence M, Roberts NJ, Ward BC, Millard TH, Clague JJ (2011) Stability analysis of the 2007 Chehalis Lake landslide based on long-range terrestrial photogrammetry and airborne-LiDAR data. Landslides. doi:10.1007/s10346-011-0286-4

Cheng D, Liu H, Lium D, Cui Z (2010) 3D deformation study on anti-dip layered rock slopes. In: Williams AL, Pinches GM, Chin CY, McMorran TJ, Massey CI (eds) 11th Congress of the international association for engineering geology and the environment. CRC Press, Auckland, New Zealand, pp 2771–2778

Choquet P, Tanon DDB (1985) Nomograms for the assessment of toppling failure in rock slopes. In: 26th U.S. symposium on rock mechanics. Rapid City, South Dakota, Balkema, Rotterdam, pp 19–30

Corkum AG, Martin CD (2004) Analysis of a rock slide stabilized with a toe-berm: a case study in British Columbia, Canada. Int J Rock Mech Min Sci 41(7):1109–1121

Cundall PA (1988) Formulation of a three-dimensional distinct element model—part I: a scheme to detect and represent contacts in a system composed of many polyhedral blocks. Int J Rock Mech Min Sci Geomech Abstr 25(3):107–116

Eberhardt E, Stead D, Coggan JS (2004) Numerical analysis of initiation and progressive failure in natural rock slopes—the 1991 Randa Rockslide. Int J Rock Mech Min Sci 41(1):69–87

Einstein HH, Veneziano D, Baecher GB, O'Reilly KJ (1983) The effect of discontinuity persistence on rock slope stability. Int J Rock Mech Min Sci Geomech Abstr 20(5): 227–236

Franz J (2009) An investigation of combined failure mechanisms in large scale open pit slopes. PhD thesis. University of New South Wales, Sydney Australia, 387 p

Franz J, Cai Y (2008) Investigation of slope failure mechanisms caused by large scale geological structures at the Cadia Hill Open Pit. In: Chen Z, Zhang J-M, Ho K, Wu F-Q, Li Z-K (eds) Proceedings of the 10th international symposium on landslides and engineered slopes. CRC Press, pp 1165–1171

Galic D, Glaser SD, Goodman RE (2008) Calculating the shear strength of a sliding asymmetric block under varying degrees of lateral constraint. Int J Rock Mech Min Sci 45(8): 1287–1305

Goodman RE (2003) A hierarchy of rock slope failure modes. Felsbau 21(2):8–12

Goodman RE, Bray JW (1976) Toppling of rock slopes. In: Specialty conference on rock engineering for foundations and slopes. American Society of Civil Engineering, Boulder, Colorado, pp 201–234

Goodman RE, Kieffer DS (2000) Behaviour of rock in slopes. J Geotech Geoenviron Eng 126(8):675–684

Hammah RE, Yacoub T, Curran JH (2009) Variation of failure mechanisms of slopes in jointed rock masses with changing scale. In: Diederichs MS, Grasselli G (eds) Third Canada-U.S. rock mechanics symposium, Toronto, Canada, Paper 3956

Hart RD (1993) An introduction to distinct element modeling for rock engineering. In: Hudson JA, Brown ET, Fairhurst C, Hoek E (eds) Comprehensive rock engineering: principles, practice and projects. Pergamon, pp 245–261

Hart RD, Cundall PA, Lemos J (1988) Formulation of a three-dimensional distinct element model—part II. Mechanical calculations for motion and interaction of a system composed of many polyhedral blocks. Int J Rock Mech Min Sci Geomech Abstr 25(3):117–125

Hencher SR, Liao Q-H, Monaghan BG (1996) Modelling slope behaviour for open-pits. Trans Inst Min Metall Sect A Min Ind 105:A37–A47

Itasca (2008) 3DEC version 4.10, Itasca Consulting Group Inc. Minneapolis, Minnesota

Jennings JE (1970) A mathematical theory for the calculation of the stability in open cast mines. In: Proceedings of planning of open pit mines, Johannesburg, South Africa, pp 87–102

Kalenchuk KS, Diederichs MS, McKinnon S (2006) Characterizing block geometry in jointed rockmasses. Int J Rock Mech Min Sci 43(8):1212–1225

Kalenchuk KS, Hutchinson DJ, Diederichs MS (2009a) Influence of shear surface geometry on deformation processes in massive landslides. In: Diederichs MS, Grasselli G (eds) 3rd Canada-US rock mechanics symposium, Toronto, Canada, Paper 3974

Kalenchuk KS, Hutchinson DJ, Diederichs MS (2009b) Downie slide—interpretation of complex slope mechanics in a massive, slope moving, translational landslide, 62nd Canadian geotechnical conference, Halifax, Canada, pp 367–374

Kieffer DS (2003) Rotational instability of hard rock slopes. Felsbau 21(2):31–38

Kieffer DS (2006) Influence of cross jointing on block slump stability. In: 41st US symposium on rock mechanics: 50 year of rock mechanics—landmark and future challenges, Golden, Colorado, pp 6–1127

Kimber OG, Allison RJ, Cox NJ (1998) Mechanisms of failure and slope development in rock masses. Trans Inst Br Geograph 23(3):353–370

Kinakin D (2004) Occurrence and genesis of alpine linears due to gravitational deformation in south western British Columbia. M.Sc. Thesis, Simon Fraser University, Burnaby, BC, 174 p

Kulhawy FH (1975) Stress deformation properties of rock and rock discontinuities. Eng Geol 9(4):327–350

MacLaughlin MM, Sitar N (1996) Kinematics of sliding on a hinged failure surface. In: Aubertin M, Mitri H (eds) Second North American rock mechanics symposium. Balkema, Rotterdam, pp 2025–2030

Nichol SL, Hungr O, Evans SG (2002) Large-scale brittle and ductile toppling of rock slopes. Can Geotech J 39:773–788

Palassi M, Ashitiani M (2008) Comparison of 2D and 3D distinct element analyses in stability of convex jointed rock slopes. In: 61st Canadian geotechnical conference and 9th joint CGS/IAH-CNC groundwater conference. Canadian geotechnical society, Edmonton, AB, pp 640–645

Rosso RS (1976) A comparison of joint stiffness measurements in direct shear, triaxial compression, and in situ. Int J Rock Mech Min Sci Geomech Abstr 13(3):167–172

Sagaseta C (1986) On the modes of instability of a rigid block on an inclined plane. Rock Mech Rock Eng 19:261–266

Sitar N, MacLaughlin MM, Doolin DM (2005) Influence of kinematics on landslide mobility and failure mode. J Geotech Geoenviron Eng 131(6):716–728

Sturzenegge M, Stead D (2012) The Palliser rockslide, Canadian rocky mountains: characterization and modeling of a stepped failure surface. Geomorphology 138(1):145–161

Wyllie DC, Mah C (2004) Rock slope engineering: civil and mining, 4th edn. Spon Press, New York

Yan M (2008) Numerical modelling of brittle fracture and step-path failure: from laboratory to rock slope scale. PhD thesis. Simon Fraser University, Burnaby, Canada, 308 p

Yan M, Stead D, Sturzenegger M (2007a) Step-path characterization in rock slopes: an integrated numerical modeling-digital imaging approach. In: Proceeding of the 11th congress of the international society for rock mechanics. Lisbon, Portugal, pp 693–696

Yan M, Elmo D, Stead D (2007) Characterization of step-path failure mechanisms: a combined numerical modelling-field based study. In: Eberhardt, E, Stead D, Morrison T (eds) 1st Canada-U.S. rock mechanics symposium. Vancouver, BC, pp 493–501

Yoon WS, Jeong UJ, Kim JH (2002) Kinematic analysis for sliding failure of multi-faced rock slopes. Eng Geol 67: 51–61